

Searching for vortex structures in high Reynolds number turbulence

S. I. Vainshtein

Department of Astronomy and Astrophysics, University of Chicago, Chicago, Illinois 60637

(November 21, 2018)

In experimental study of very high Reynolds number turbulence, we found evidences that there are distinguished vortex structures in the intermediate range, that is, between the Kolmogorov and Taylor microscales, where they are indeed expected to be present. These structures are responsible for the intermittency, and, in the same time, they contribute into asymmetry of turbulent statistics, the latter following from the Kolmogorov law.

PACS number(s): 47.27.Ak, 47.27.Jv

I. INTRODUCTION

The presence of organized structures in fully developed turbulence was demonstrated recently both in physical experiments, and in numerical simulations. Most of the studies are devoted to vortex tubes (or “worms”, or “sinews”), see, e.g., [1]– [6].

Generally, these organized structures may be considered at the same time as a source (or manifestation) of intermittency, because normally they correspond to a small dimension (of the size of Taylor microscale, or Kolmogorov microscale), although they are stretched in the other directions over a “macroscopic” length.

One remarkable feature of these vortex structures is that they present not only the intermittency of turbulence, but also contribute into the asymmetry of the PDF’s [3], [4]. As was suggested in [7], the asymmetric statistics of the turbulence is indeed related to the intermittency. This connection was summarized in the so-called ramp-model, the latter being only empirical. The considerations of the formation of vortex structures, when the intermittency and asymmetry appear simultaneously, have resulted in the development of the ramp-model into a more sophisticated version which is now called the bump-model.

The data used in this paper are based on Taylor’s hypothesis, and therefore do not provide direct measurements of vortices. However, these vortices should be manifested in different ways, such as appearance of intermittency, etc. We provide here evidences that these vortices are present in fully developed turbulence. We believe that the disadvantages of necessary indirect studies of vortices presented in this paper, are outweighed by the fact that we are studying a very high Reynolds turbulence.

The paper is organized as follows. Section II is still introductory, presenting (mostly known) notions of turbulence statistics, related to the vortices. The main purpose of this section is to explain, what can we expect to observe from experimental data if the vortices are present, and also to introduce denotations we will use in the rest of the paper; and thus some repetition of previous results seems to be inevitable. On the other hand, the bump-

model is introduced in Sec. II B. Section III starts with suggestions how to improve the two extreme cases, or models, considered in Sec. II. The answer is in the middle: an intermediate model is suggested. The rest of the section is devoted to comparison of this model with the experimental data, namely, with the observed structure functions of low orders. Section IV presents evidences of existing vortices. Namely, it is shown that the intermittency is substantially enhanced in the intermediate range: from studying the flatness of the velocity increments statistics, Sec. IV A, and from the box counting, Sec. IV B. An extensive discussion of both extreme case models, and also of the intermediate model is given in Sec. V. It is argued that this model may give an insight into the question of the intermittency formation, which proves to be intimately connected with the asymmetry of turbulence. Finally, concluding remarks are presented in Conclusion, Sec. VI.

II. BASIC IDEAS AND DENOTATION

We consider structure functions,

$$\mathcal{S}_n(r) = \langle (\Delta_r u)^n \rangle, \quad (1)$$

where $\Delta_r u = u(x+r) - u(x)$, and n is an integer, and generalized structure functions,

$$\mathcal{S}_q(r) = \langle |\Delta_r u|^q \rangle, \quad (2)$$

where $q > 0$.

We mention an exact result, obtained directly from Navier-Stokes equation,

$$\mathcal{S}_3(r) = -\frac{4}{5}\varepsilon r + 6\nu \frac{\partial}{\partial r} \mathcal{S}_2(r), \quad (3)$$

[8], and in inertial range where the viscosity term can be neglected, we recover the 4/5-Kolmogorov law,

$$\mathcal{S}_3(r) = -\frac{4}{5}\varepsilon r. \quad (4)$$

Data are from atmospheric turbulence measurements, about 35 meters above the ground, obtained by hot-wire anemometer, mean wind speed was 7.6 m/sec, root-mean-square velocity 1.3 m/sec. Using Taylor's hypothesis and local isotropy assumption to obtain dissipation, one obtains the Taylor microscale Reynolds number to be 9540 and the Kolmogorov microscale η to be 0.57 mm. The data were sampled at 5 kHz and the file consisted of 10 million data points (courtesy of Sreenivasan). The data are treated in the spirit of the Taylor hypothesis, that is, the time series is treated as one-dimensional cut of the process (for more detail, see [9–11]).

A. No intermittency. Asymmetry in K41

Consider classical picture of turbulence due to K41 [12]. That is, the turbulence is presented with an ensemble of multiscale cells, from integral scale ℓ to smallest Kolmogorov scale $\eta \sim \ell/R^{3/4}$, where $R \approx v\ell/\nu$, the Reynolds number, and $v = \sqrt{\langle v_x^2 + v_y^2 + v_z^2 \rangle}$, the mean square velocity, with $|\Delta_r u| \sim r^{1/3}$. Then, in inertial range, i.e., at $\eta < r < \ell$,

$$S_q(r) \sim r^{q/3}. \quad (5)$$

We define the Taylor microscale,

$$\lambda = \sqrt{\frac{\langle u^2 \rangle}{\langle (\partial_x u)^2 \rangle}}, \quad (6)$$

see, e.g., [13]. Then,

$$\lambda \sim \frac{\ell}{R^{1/2}}, \quad \text{and} \quad R_\lambda = \frac{\langle u^2 \rangle^{1/2} \lambda}{\nu} \sim R^{1/2}. \quad (7)$$

It follows from (6) that

$$\lambda = 15^{1/4} \eta R_\lambda^{1/2}, \quad (8)$$

see, e.g., [14], formula (3.2.18), we use this expression below.

Let us proceed to the asymmetry, dictated by the Kolmogorov law (4). Denote $\lambda_{1,2,3}$ – three eigen values of the symmetric part of the matrix $\partial_j v_i$, and suppose that

$$\lambda_1 \leq \lambda_2 \leq \lambda_3. \quad (9)$$

It is known [15], that the quantity defining skewness of $\partial_x u$ field, namely $\langle (\partial_x u)^3 \rangle$, is $= (8/35)\langle \lambda_1 \lambda_2 \lambda_3 \rangle$, and therefore we calculate $\langle \lambda_1 \lambda_2 \lambda_3 \rangle$. As $\lambda_1 + \lambda_2 + \lambda_3 = 0$ (due to the incompressibility), (9) can be replaced by

$$-\frac{\lambda_3}{2} \leq \lambda_2 \leq \lambda_3. \quad (10)$$

We thus consider conditional mean value (λ_3 is fixed)

$$\langle \lambda_1 \lambda_2 \lambda_3 | \lambda_3 \rangle = -\langle (\lambda_2 + \lambda_3) \lambda_2 \lambda_3 \rangle =$$

$$\int_{-\lambda_3/2}^{\lambda_3} p(\lambda_2 | \lambda_3) [-(\lambda_2 + \lambda_3) \lambda_2 \lambda_3] d\lambda_2, \quad (11)$$

where $p(\lambda_2 | \lambda_3)$ is conditional probability distribution of λ_2 . The quantity $\lambda_1 \lambda_2 \lambda_3$ as a function of λ_2 is highly asymmetric and mostly negative in the range (10). If, for example, we suppose that $p(\lambda_2 | \lambda_3)$ is an uniform distribution, i.e.,

$$p(\lambda_2 | \lambda_3) = \frac{1}{(3/2)\lambda_3},$$

which at first sight seems to be quite a realistic assumption, then, according to (11), $\langle \lambda_1 \lambda_2 \lambda_3 | \lambda_3 \rangle = -\lambda_3^3/2 < 0$. In fact, the contribution of the negative part of $\lambda_1 \lambda_2 \lambda_3$ is 10 times larger than the positive part; that is, in order to make the integral in (11) positive, the distribution $p(\lambda_2 | \lambda_3)$ should be highly asymmetric. Namely, $p(\lambda_2 | \lambda_3)$ should be more than 10 times larger in the negative range of (10) than in the positive. As this kind of assumption concerning the PDF $p(\lambda_2 | \lambda_3)$ does not seem to be reasonable, it follows from these considerations that $\langle (\partial_x u)^3 \rangle$, and therefore the skewness should be negative.

In a more natural way, one may consider the strain parameter,

$$\tilde{\lambda} = \frac{\lambda_1 - \lambda_2}{\lambda_1 + \lambda_2} = \frac{2\lambda_2 + \lambda_3}{\lambda_3},$$

introduced by Moffatt et al. [2], and, according to (10), $0 \leq \tilde{\lambda} \leq 3$. Then,

$$\lambda_1 \lambda_2 \lambda_3 = \frac{\lambda_3^3}{4} (1 - \tilde{\lambda}^2).$$

The interval where this expression is positive (i.e., $0 \leq \tilde{\lambda} < 1$) is twice as short as where it is negative (i.e., $1 < \tilde{\lambda} < 3$), and therefore the mean value may be expected to be negative. And indeed, for an uniform PDF $p(\tilde{\lambda} | \lambda_3) = 1/3$, we recover

$$\langle \lambda_1 \lambda_2 \lambda_3 | \lambda_3 \rangle = \frac{\lambda_3^3}{4} \int_0^3 p(\tilde{\lambda} | \lambda_3) (1 - \tilde{\lambda}^2) d\tilde{\lambda} = -\lambda_3^3/2 < 0.$$

These considerations appear to be “too general”, and therefore suspicious, because they do not incorporate the equation of motion. And indeed, these considerations are bias. Recall that λ_3 (which is > 0) was previously fixed; if we now fix $\lambda_1 (< 0)$, then

$$\lambda_1 \leq \lambda_2 \leq -\frac{\lambda_1}{2}, \quad (12)$$

cf., (10). Calculating now $\langle \lambda_1 \lambda_2 \lambda_3 | \lambda_1 \rangle = -\langle \lambda_1 \lambda_2 (\lambda_1 + \lambda_2) \rangle$, analogously to (11), we obtain $\langle \lambda_1 \lambda_2 \lambda_3 | \lambda_1 \rangle = -\lambda_1^3/2 > 0!$

Finally, if we no longer require (9), i.e., if we do not require any ordering for the eigen values, then $\langle \lambda_1 \lambda_2 \lambda_3 \rangle = 0$. Indeed, all probability distributions are expected to

be symmetric *a priori* in respect to the transformation $\lambda_{1,2,3} \rightarrow -\lambda_{1,2,3}$, and therefore $\langle \lambda_1 \lambda_2 \lambda_3 \rangle = 0$. Thus, these “general considerations” fail to account for the asymmetry, because they do not incorporate the equation of motion. In the framework of K41, the asymmetry *is needed* to account for the energy transfer to small eddies [13], the asymmetry by itself being expressed through the Kolmogorov law (4). However, the theory does not indicate what dynamical processes lead to the asymmetry. Another setback in this picture is that the turbulence is completely non-intermittent, in contradiction with experimental data.

In particular, the asymmetry dictated by the Kolmogorov law, and observed (negative) skewness, are not supposed to be related to the intermittency. That is, the PDF for $\Delta_r u$ is asymmetric, however, the asymmetry has nothing to do with the tails of the PDF, that is with possible intermittency. In other words, the asymmetry of the PDF is expected to be manifested in the core. This “ideal” PDF is constructed in [11], in order to compare with observed properties of turbulence. The PDF,

$$p(\tilde{u}, r) \equiv \mathcal{I}(\tilde{u}), \quad \tilde{u} = \frac{\Delta_r u}{\langle (\Delta_r u)^2 \rangle^{1/2}} \quad (13)$$

has the following properties,

$$\int \mathcal{I}(\tilde{u}) d\tilde{u} = 1, \quad \int \tilde{u} \mathcal{I}(\tilde{u}) d\tilde{u} = 0, \quad \int \tilde{u}^2 \mathcal{I}(\tilde{u}) d\tilde{u} = 1,$$

and

$$\int \tilde{u}^3 \mathcal{I}(\tilde{u}) d\tilde{u} = -\frac{4}{5} \frac{1}{C_2^{3/2}}, \quad (14)$$

where C_2 is the Kolmogorov constant. But, most importantly, the PDF is constructed from two Gaussian functions, so that it does not contain any tails. We will use this “ideal” PDF below; we note for now that the experimental asymmetry *is* related to the intermittency. In particular, the tails of real PDF give a substantial contribution to the Kolmogorov law [11].

In addition, the experimental PDF $p(\tilde{u}, r)$ is not self-similar, that is, it is also a function of r (as well as of \tilde{u} , cf. (13)), see, e.g., [9]. This in effect implies presence of intermittency. Direct study of intermittency can be provided by cumulative moments,

$$S_{0,c}(r) = \int_{-c}^c p(\tilde{u}, r) d\tilde{u}, \quad (15)$$

and

$$S_{-,c}(r) = \int_{-c}^0 p(\tilde{u}, r) d\tilde{u}, \quad S_{+,c}(r) = \int_0^c p(\tilde{u}, r) d\tilde{u}, \quad (16)$$

and by the tail moments,

$$S_{0,t}(r) = \int_{-\infty}^{-t} p(\tilde{u}, r) d\tilde{u} + \int_t^{\infty} p(\tilde{u}, r) d\tilde{u} = 1 - S_{0,c=t}(r), \quad (17)$$

and

$$S_{-,t}(r) = \int_{-\infty}^{-t} p(\tilde{u}, r) d\tilde{u}, \quad S_{+,t}(r) = \int_t^{\infty} p(\tilde{u}, r) d\tilde{u}. \quad (18)$$

If c and t are not small (we will consider $c = t = 3$, and $c = t = 4$), then (15) presents major events produced by the core of the PDF, and $S_{0,c}$ should be close to unity, or rather Gaussian value with which it will be compared. We denote the cumulative and tail moments for Gaussian and “ideal” distributions with letters G and \mathcal{I} correspondingly. For example, $S_{0,c}(r)$ for Gaussian distribution is $G_{0,c}$, and $S_{-,t}(r)$ for ideal distribution is $\mathcal{I}_{-,t}$, etc. And, of course, $S_{0,c}$ should be independent of r , in case of self-similarity. On the contrary, substantial deviation from unity, and, what is more important, dependence on the distance – increasing with growing r , would indicate intermittency. In fact, super-Gaussian deviation from unity suggests that the tails give considerable contribution to the PDF, and this contribution is decreasing with growing distance. We will see in Sec. IV B that that is what is indeed observed.

As to $S_{\pm,c}(r)$, they represent a more subtle way to measure intermittency, and, of course, asymmetry. These quantities are expected to be close to (and smaller than) $1/2$, and $S_{+,c}$ being slightly larger than $S_{-,c}$.

B. Extreme intermittency

There is a geometrical interpretation of $\langle \lambda_1 \lambda_2 \lambda_3 \rangle < 0$. It implies that typically $\lambda_1 < 0$, while $\lambda_{2,3} > 0$, that is, the inflow is in one direction, 1, while the outflow proceeds in two directions, 2,3. Statistically, these flows would generate vortex sheets rather than vortex ropes [16]. However, it became clear that the presence of the vortex itself changes the principal axes and eigen values [3,4]. Consider an axisymmetric cell of a scale ℓ . At the axis, there is an inflow in two directions, 1,2, that is, to the axis, and outflow in one direction, 3, parallel to the axis. Therefore, locally $\lambda_1 \lambda_2 \lambda_3 > 0$ ($\lambda_{1,2} < 0$ and $\lambda_3 > 0$). To be more specific, in cylindrical coordinates $\{r', \phi, z\}$,

$$\mathbf{v} = \{ -\alpha r', \quad 0, \quad 2\alpha z \}, \quad (19)$$

$\alpha = -\lambda_1 = -\lambda_2 = \lambda_3/2$. Suppose now that there is a symmetric vortex present, with initial scale ℓ . Then the vortex is stretched by the strain motion (19), according to equation

$$\partial_t \omega_z - \alpha r' \partial_{r'} \omega_z = 2\alpha \omega_z + \frac{\nu}{r'} \partial_{r'} r' \partial_{r'} \omega_z. \quad (20)$$

This stretching proceeds until viscous effects come into play, resulting in Burgers vortex,

$$\omega_z(r') = \omega_z(0) e^{-r'^2/\lambda^2}, \quad (21)$$

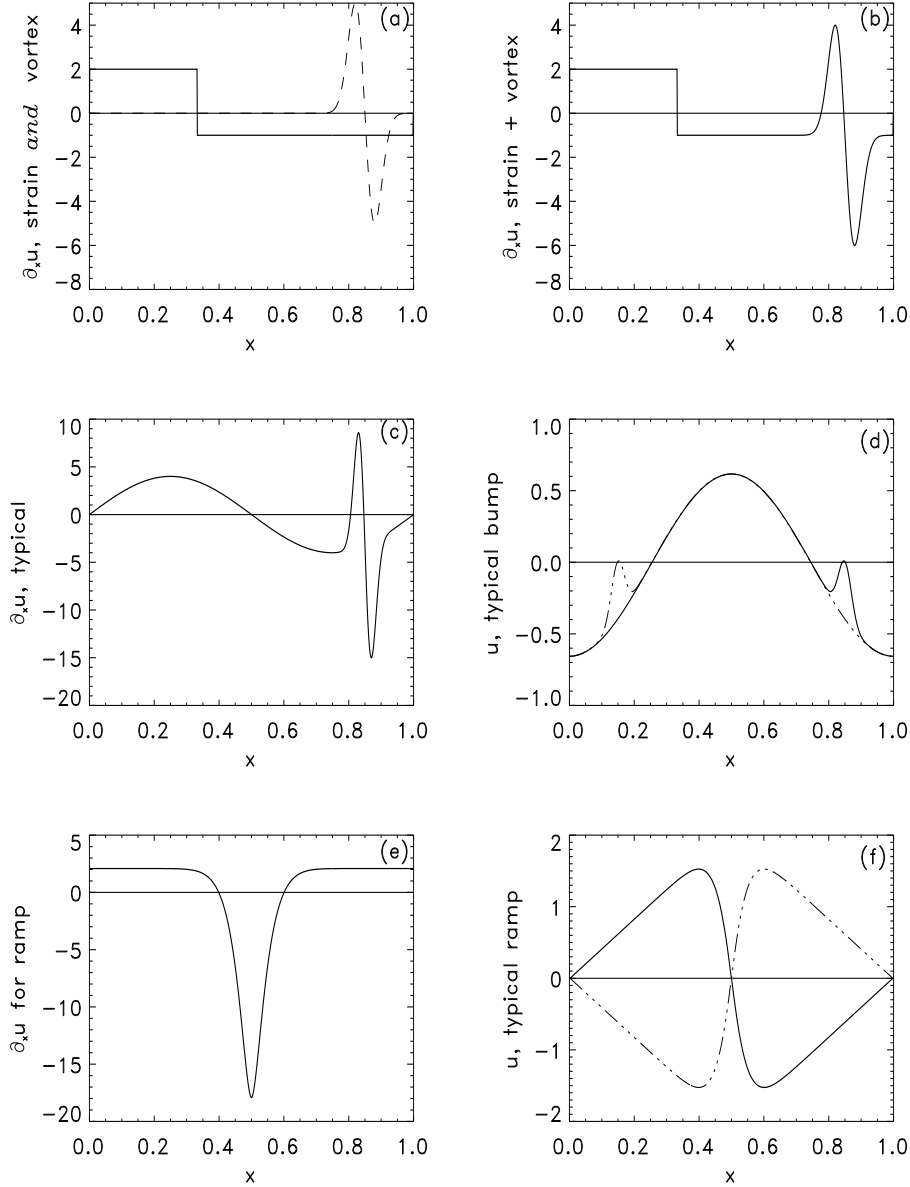


FIG. 1. Schematic presentation of bump model, and its comparison with the ramp-model. (a) Presentation of $\partial_x u$ for the strain (19), solid line. The vortex is superimposed on this plot (dashed line). (b) Resulting motion, the strain plus the vortex. (c) More realistic presentation of the same as in (b). (d) Corresponding motion u . Note typical bump. The dashed-dotted line presents a bump in a “wrong place”, that is, this situation is statistically unlikely. (e) $\partial_x u$ for the ramp-model, and (f), corresponding motion, which is indeed ramp-like. The dashed-dotted line depicts another ramp, which is supposed to appear statistically rarely.

and

$$v_\phi = \frac{\omega_z(0)\lambda^2}{2r'} \left(1 - e^{-r'^2/\lambda^2}\right), \quad (22)$$

where

$$\lambda = \sqrt{\frac{2\nu}{\alpha}}. \quad (23)$$

As $\alpha \sim v_\ell/\ell$, $\lambda \sim \ell R^{-1/2}$, and therefore λ coincides with Taylor microscale (7). In order to estimate $\omega_z(0)$ we note that, neglecting viscosity, equation (20) conserves the quantity

$$\int \omega_z r' dr', \quad (24)$$

and hence we estimate, $\omega_z \sim 1/r'^2$, that is,

$$\omega_z(0) \approx \omega_\ell \frac{\ell^2}{\lambda^2} = \omega_\ell R, \quad (25)$$

where ω_ℓ is initial vorticity.

It was shown in [3,4] that the combination of the strain motion (19) and the vortex results in negative skewness. In order to get some simple estimates, we present $\partial_x u$ corresponding to this motion in Fig. 1. Figure 1(a) presents the strain (19) with $\alpha = 1$. The probability $p(\partial_x u > 0) = 1/3$ (where $\partial_x u = 2$), while $p(\partial_x u < 0) = 2/3$ (and $\partial_x u = -1$), and therefore

$$\langle \partial_x u_{st} \rangle = 2p(\partial_x u > 0) - 1p(\partial_x u < 0) = 0,$$

and

$$\langle (\partial_x u_{st})^3 \rangle = 8p(\partial_x u > 0) - 1p(\partial_x u < 0) = 8/3 - 2/3 = 2 > 0.$$

That is, the skewness is positive for the strain motion, as mentioned above. The vortex corresponds to a sharp odd function concentrated on a small scale λ . Therefore, $\langle \partial_x u_\lambda \rangle = 0$ and $\langle (\partial_x u_\lambda)^3 \rangle = 0$. Nevertheless, the sum of these motions, depicted in Fig. 1(b), may possess negative skewness. Indeed,

$$\langle \partial_x u_{st} + \partial_x u_\lambda \rangle = \langle \partial_x u_{st} \rangle + \langle \partial_x u_\lambda \rangle = 0,$$

while

$$\langle (\partial_x u_{st} + \partial_x u_\lambda)^3 \rangle = \langle (\partial_x u_{st})^3 \rangle - 3 \cdot 1 \langle (\partial_x u_\lambda)^2 \rangle \quad (26)$$

(cf. [4]), which becomes negative if the second term on the right-hand-side prevails. In particular, for the strain (19) plus vortex (21),

$$\langle (\partial_x u_{st} + \partial_x u_\lambda)^3 \rangle = 2\alpha^3 - 3\alpha\omega_\ell^2 R^2 \frac{\lambda^2}{\ell^2} \approx -3\alpha\omega_\ell^2 R, \quad (27)$$

where we used the estimate (25), and the fact that the vortex occupies only λ^2/ℓ^2 part of the space (naturally, we also suppose that ω_ℓ is not small compared with α).

Figure 1(c) depicts essentially the same as Fig. 1(b), but it suggests a more realistic presentation of $\partial_x u$. The integral of this latter function, that is, the velocity u itself is depicted in Fig. 1(d). Note characteristic bump which appears due to the vortex. Panels (e) and (f) are to be compared with (c) and (d); they present $\partial_x u$ and u for the ramp model (the details of this comparison are given in Secs. IV B and V A).

Imagine now a statistical ensemble of the cells of the scale ℓ , so that the ensemble as a whole is statistically isotropic. Suppose that each of the cells contains a Burgers vortex (21) with $\omega_\ell \approx \alpha$. Then,

$$\langle (\partial_x u)^2 \rangle \sim \omega_\ell^2 R^2 \frac{\lambda^2}{\ell^2} \sim \omega_\ell^2 R \sim \left(\frac{v_\ell}{\ell}\right)^2 R, \quad (28)$$

so that

$$\nu \langle (\partial_x u)^2 \rangle \sim \frac{v_\ell^3}{\ell} \sim \varepsilon, \quad (29)$$

as in K41 theory.

The Kolmogorov law (4) is also valid, of course. However, the ‘‘inertial range’’ for this ensemble, starting at the scale ℓ is cut off already at the Taylor microscale λ , rather than Kolmogorov microscale η , because the linear in r term in (3) is larger than the viscous term only at $r > \lambda$. At $r < \lambda$ $\mathcal{S}_3(r) \sim r^3$, reaching at $r = \lambda$ the amplitude $\mathcal{S}_3(\lambda) \sim \varepsilon\lambda$, as should be according to (4). In addition, the skewness, $\sim \mathcal{S}_3(\lambda)/\lambda^3 \sim -\varepsilon/\lambda^2 \approx -(v_\ell/\ell)^3 R$, which coincides with the estimate (27).

So far, this ensemble looks similar to the K41 theory. However the intermittency in this model is much too high. For example, $\langle (\partial_x u)^4 \rangle \sim \omega_\ell^4 R^4 \lambda^2/\ell^2 \sim \omega_\ell^4 R^3$, so that the flatness,

$$F(0) = \frac{\langle (\partial_x u)^4 \rangle}{\langle (\partial_x u)^2 \rangle^2} \sim R, \quad (30)$$

which is many orders of magnitude above the experimental value (see, e.g., below Sec. IV A).

III. COMPARISON WITH EXPERIMENTAL DATA

Further discussion of these two models and the ramp model is provided below in Sec. V. It is clear for now that both extreme cases: no intermittency II A, and extreme intermittency II B are not realistic, and it should be accepted something in between. Let us accept the K41 theory as a ‘‘first approximation’’, and we will try to modify it by introducing finite intermittency. Then, in addition to what is described in Sec. II A, the cells are generating vortices as in Sec. II B above. The question is, what are the initial magnitudes of ω_r ? It is clear that, for example, ω_ℓ should be small compared with v_ℓ/ℓ : otherwise the intermittency is too strong. Another possibility is to suggest that $\omega_\ell \sim v_\ell/\ell$, however, only a small

fraction of the cells are generating these vortices. In addition, there is nothing special in the large scale eddies; in fact, the cells with scales $r < \ell$ are generating the vortex ropes as well. Namely, the scales of generated vortices by the cells of the scale r are,

$$\delta_r = \sqrt{\frac{2\nu}{v_r/r}} = \lambda \left(\frac{r}{\ell}\right)^{1/3}, \quad (31)$$

cf. (23). Each cell is able to generate a vortex rope as long as $\delta_r < r$, i.e., according to (31), when $r > \ell/R^{3/4} \sim \eta$, that is, in the whole inertial range. Thus, the vortices are generated in each cell, however, the scales of these vortices, δ_r , are,

$$\eta \leq \delta_r \leq \lambda. \quad (32)$$

We can call this range intermediate, and it is in this range where the vortices are indeed observed [5].

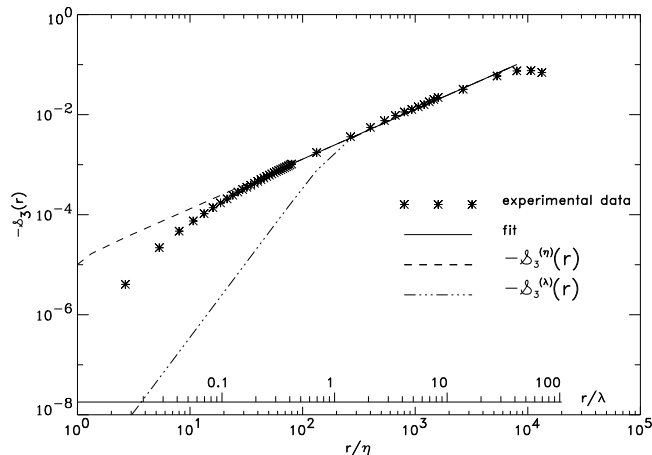


FIG. 2. Experimental and theoretical (somewhat simplified and sketchy) third moment, $\mathcal{S}_3(r)$.

We note that, according to Sec. II B, the vortex is stretched along the stretching axis (with maximum value of $\lambda_{1,2,3}$), of course, that is, parallel to the z -axis. However, as mentioned at the beginning of Sec. II B, when the vortex is formed, the eigen values are changed. While λ_3 remains the same $= 2\alpha$, the other two eigen values are now

$$\lambda_{1,2} \rightarrow -\alpha \pm \frac{1}{2} \left| \frac{dv_\phi}{dr'} - \frac{v_\phi}{r'} \right|,$$

where v_ϕ is defined in (22), see, e.g., [4]. We now have to arrange the eigen values in order (9) to obtain

$$\lambda_1 = -\alpha - \frac{1}{2} \left| \frac{dv_\phi}{dr'} - \frac{v_\phi}{r'} \right|, \quad \lambda_2 = 2\alpha, \quad (33)$$

$$\lambda_3 = -\alpha + \frac{1}{2} \left| \frac{dv_\phi}{dr'} - \frac{v_\phi}{r'} \right|.$$

We see that now the vortex is aligned along the *intermediate* eigenvector. This feature was initially suggested and shown in [6], and confirmed both in numerical simulations [5], and in laboratory experiments [17].

In addition, the eigen values (33) result in correct sign of the skewness (i.e., correct asymmetry of the PDF). Indeed,

$$\lambda_1 \lambda_2 \lambda_3 = 2\alpha \left[\alpha^2 - \frac{1}{4} \left(\frac{dv_\phi}{dr'} - \frac{v_\phi}{r'} \right)^2 \right] < 0,$$

if the amplitude of the vortex is large enough. This formula is consistent with the estimate (27). Indeed, $dv_\phi/dr' - v_\phi/r' \approx \omega_\ell R^2$, and averaging this expression over the space would result in a factor $\sim 1/R$, because the vortex is occupying only $1/R$ fraction of space. As a result, we recover (27).

A. The third moment

In order to understand what impact has this model on the structure functions, we start with the third order structure function. As mentioned, for the extreme intermittency case, Sec. II B, $\mathcal{S}_3 \sim r^3$ for $r < \lambda$, while for no-intermittency case, Sec. II A, $\mathcal{S}_3 \sim r^3$ is valid for $r < \eta$. Naturally, the picture outlined above in this section suggests intermediate situation.

Figure 2 depicts experimental $\mathcal{S}_3(r)$, and it is compared with what we would expect for the ensemble described in Sec. II B, namely, with the following function constructed for this purpose

$$\mathcal{S}_3^{(\lambda)}(r) = -\frac{4}{5} r \varepsilon \tanh \left(\frac{r}{\lambda} \right)^2.$$

The experimental $\mathcal{S}_3(r)$ is also compared with

$$\mathcal{S}_3^{(\eta)}(r) = -\frac{4}{5} r \varepsilon \tanh \left(\frac{r}{\eta} \right)^2,$$

which is what one would expect from K41. Note that all three curves, one experimental and two constructed, match at inertial range, i.e., at $r > \lambda$. In order to do this, the constructed functions are matching experimental linear fit with exponent $\zeta_3 = 0.99 \pm 0.01$, quite close to the Kolmogorov law (for which $\zeta_3 = 1$). The plots are given in Kolmogorov microscale, that is, in r/η , and there is also r/λ scale in the figure for comparison. It can be seen that the inertial range indeed starts at $r \approx \lambda$, and thus the intermediate range (32) is clearly visible. Besides, the experimental plot is situated between no intermittency moment, $\mathcal{S}_3^{(\eta)}(r)$, and extreme intermittency, $\mathcal{S}_3^{(\lambda)}(r)$, – as expected.

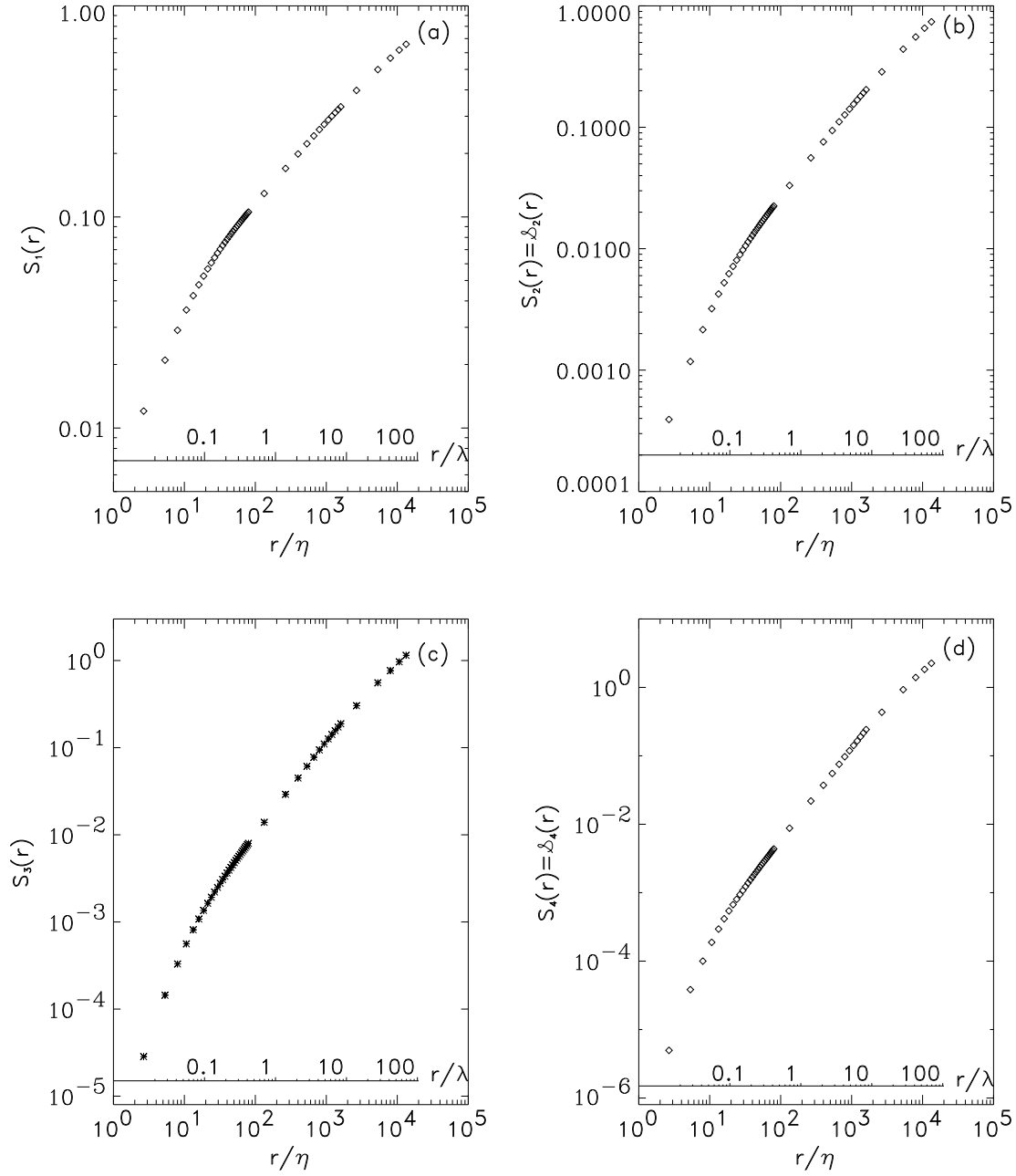


FIG. 3. Panels (a) through (d): the generalized structure functions: starting from the first and ending with the fourth.

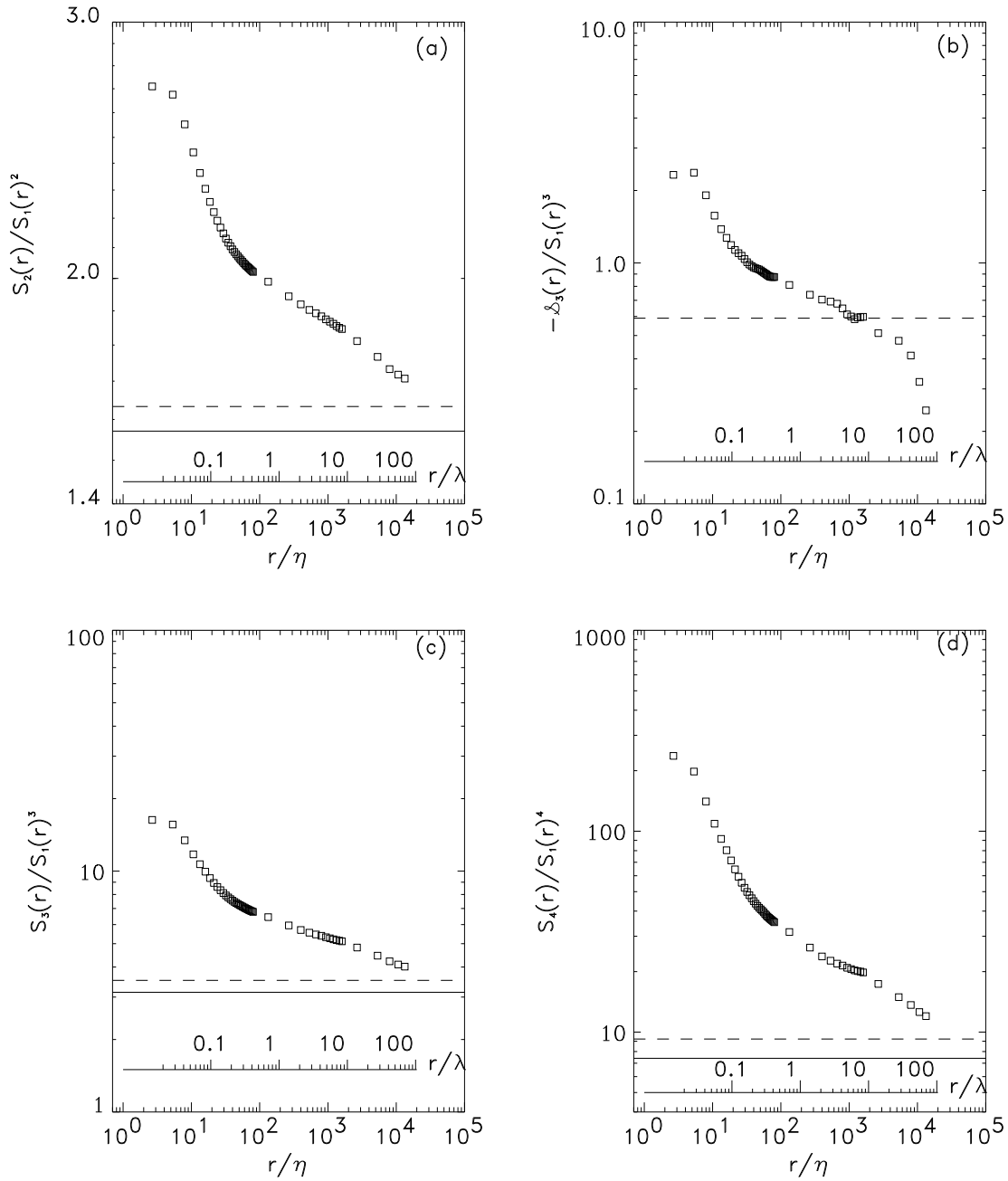


FIG. 4. Generalized flatness; several dimensionless ratios of different moments to the first. The plots are compared with the Gaussian value (solid line), and with what would follow from the “ideal” PDF, see (13-14). Note that all plots are in log-log scale. The ordinate in panel (a) is in log-scale as well; it seems indistinguishable from linear scale because the scale range is relatively small.

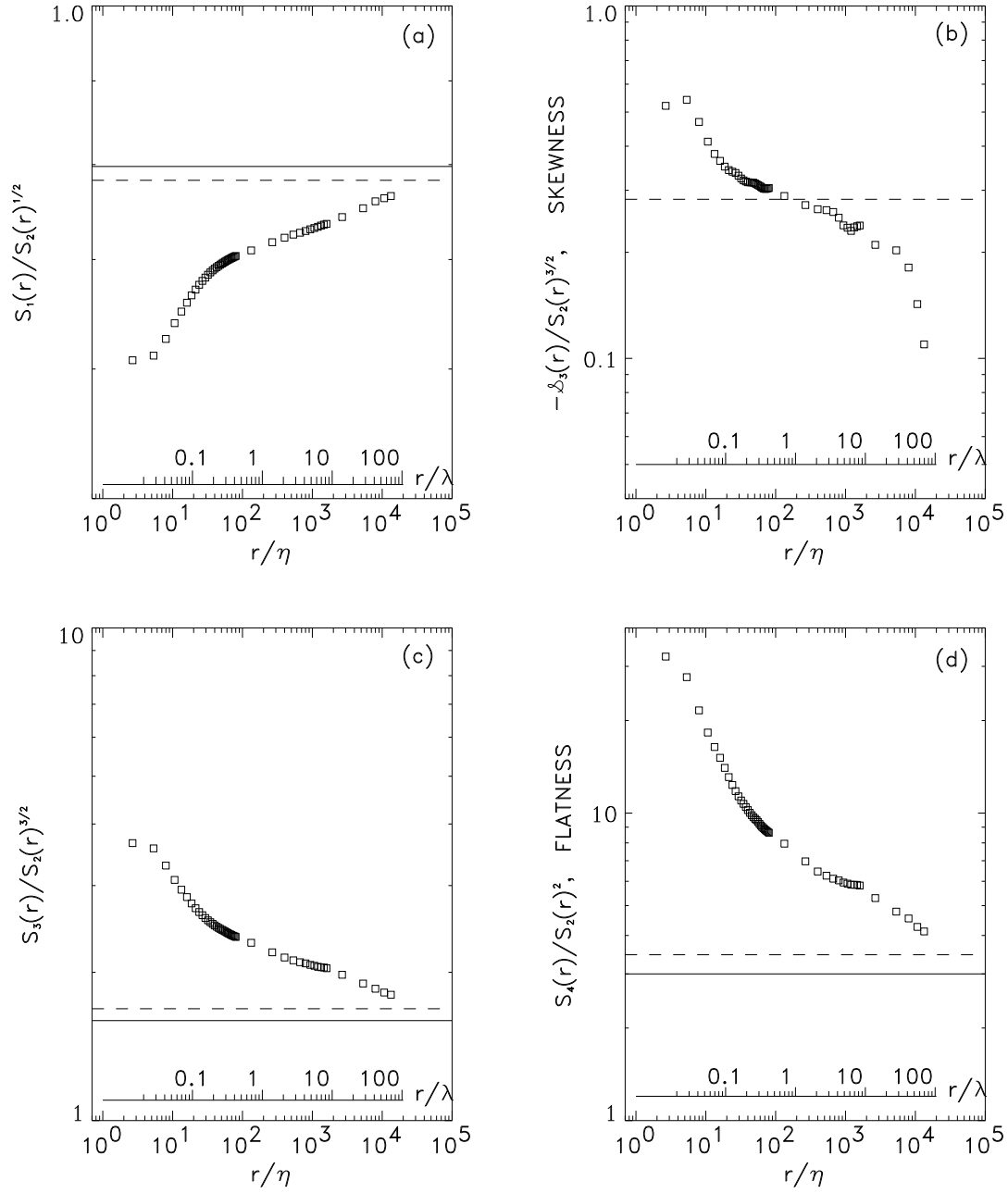


FIG. 5. Same as in previous figure, only these are ratios of moments to the second order structure function.

B. Other moments

The inertial range is associated with scaling, that is, in the log-log plotting the moments are presented with straight lines. Figure 3 illustrates generalized structure functions of different orders, the first, the second, the third and the fourth (and, of course, the structure functions of even orders coincide with the generalized structure functions). The intermediate range (32) is easily separated from the inertial range (where the plots become straight lines).

We may interpret this separation of the intermediate range by the fact that this range contains vortices. This interpretation is not unequivocal however. It is also possible that the depletion of the structure functions in this range, as compared with the K41, is due to the action of viscosity. Indeed, the viscosity is still acting even at $r \gg \eta$, in spite of the fact that the local Reynolds number is there $\gg 1$. The fact that the viscous effect is stretched up to $r \sim \lambda$ might be purely coincidental.

IV. INTERMITTENCY

A. Flatness

A real test to check if the intermediate range is related to vortices is achieved by the measuring the intermittency. Traditionally, the later is estimated by measuring the flatness, see, e.g., [13]. More specifically, the flatness, and related quantities, like generalized flatness, are compared with corresponding Gaussian values. Figure 4 presents dimensionless ratios of different moments to the first moment. They can be called generalized flatness. We see that, first, the intermediate range is clearly distinguished from inertial, the intermittency growing substantially in the intermediate range. The deviation from Gaussian and “ideal” behavior is especially dramatic in Fig. 4(d), which is hardly surprising taking into account that it represents a relatively high moment.

Second, although the deviation from Gaussian and “ideal” values in inertial range is not big, (a factor of 2 or 3), there is a noticeable scaling for about two decades. Recall that in the framework of K41, according to (5), all these ratios would be flat, that is, e.g., $S_2(r)/S_1(r)^2 = \text{const}$, etc. If however the structure functions have anomalous scaling, $S_q(r) \sim r^{\zeta_q}$, where $\zeta_q \neq q/3$, then these ratios would possess some scaling, which is indeed observed.

Finally, what may be called generalized skewness, depicted in Fig. 4(b), is presented by rather scattered curve. This might be explained as follow. The third moment of the structure function, appearing only due to the asymmetry (as opposed to the third order generalized structure function, depicted in panel (c)), contains quite a substantial contribution coming from the PDF tails, see, e.g., [10]. As the tails correspond to rare (but

stormy) events, the odd order structure functions are subject to substantial fluctuations.

Essentially the same conclusions can be drawn from analyzing Fig. 5, where the dimensionless ratios of different moments to the second order structure function are depicted. It is clear that the intermittency is substantially increased in the intermediate range. In particular, for the ratio $S_1(r)/S_2(r)^{1/2}$, the presence of intermittency implies that the ratio is *below* the Gaussian value, see Fig. 5(a), rather than otherwise for higher moments; and still, the intermediate range is clearly distinguished by enhanced intermittency. It is also clear from panel (b) that the skewness substantially exceeds that given by the “ideal” PDF only in the intermediate range. In the inertial range, the skewness is decreasing systematically with increasing distance r , although the deviation from “ideal” behavior is not conspicuous (and the scaling, if any, is rather poor). Finally, maximal flatness (panel (d)) reaches the value 32.28, well below what would be expected from extreme intermittency model described in Sec. II B.

B. Box counting

Zerth moment of structure function, that is box counting, are very useful to study because, unlike high moments, the statistic is as good as one can get, although quite often the zeroth moment provides only trivial results. In order to extract some useful data in studying intermittency, one can either analyze the cumulative (and tail) moments, or separate negative values from the positive, and to study them separately (as, e.g., in [11]).

Panel (a) and (b) in Fig. 6 correspond to experimental cumulative and tail moments, defined in (15) and (16) correspondingly, and we compare them with theoretical values. As mentioned in Sec. II A, for self-similar PDF’s, the cumulative moments are independent of distance r , and they are expected not to deviate much neither from Gaussian nor from “ideal” asymmetric distribution, - these two happen to be close to each other, as seen from panel (a). On the other hand, the contribution of the tails, that is, intermittency, if present, is increasing with decreasing distance. That implies that the cumulative moments, that is, the cores of the PDF’s give a smaller contribution for decreasing distances. Figure 6(a) shows that this is indeed the case. It can be seen that, first, the cumulative moments noticeably deviate from both Gaussian and “ideal” values. Second, this deviation is higher in the intermediate range, and that is the way this range is easily separated from the inertial range. One can see analogous trends from panel (b), where tail moments are depicted. The tails definitely give larger contribution for small distances, and this is especially true for the intermediate range, which is again noticeable. Note also that the tail parts for $t = 4$ are substantially larger than Gaussian values, especially for

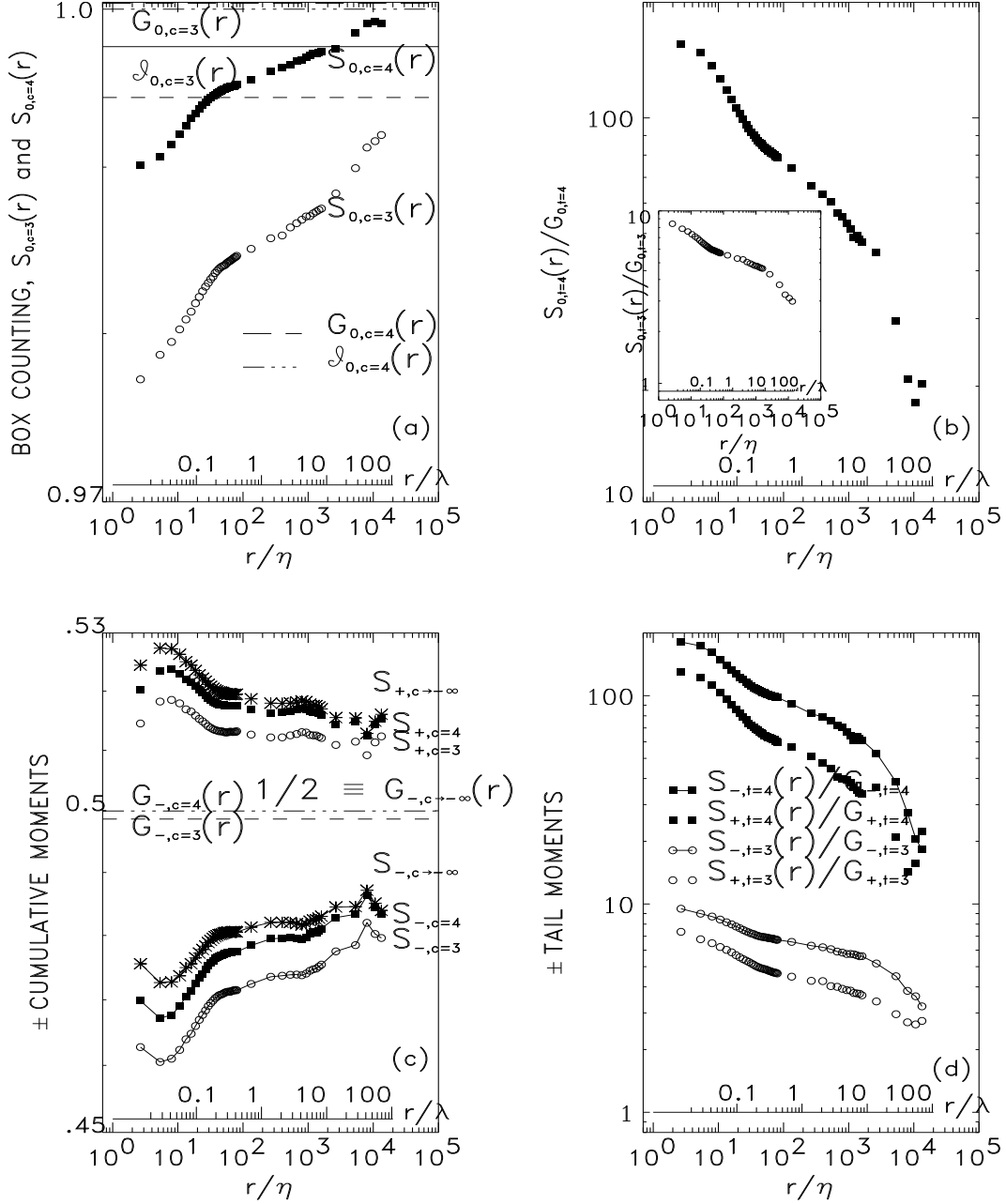


FIG. 6. Cumulative and tail moments of zeroth order. (a) The probability of $|\tilde{u}| \leq 3$, and of $|\tilde{u}| \leq 4$ for different r 's, which coincide with $S_{0,c=3}(r)$ and $S_{0,c=4}(r)$ correspondingly. These quantities are compared with correspondent Gaussian and “ideal” values, $G_{0,c=4}$ being almost indistinguishable from unity. (b) Tail moments, with respect to correspondent Gaussian values, and for the same values $t = 3$ and $t = 4$, are depicted. (c) The probability of $\tilde{u} < 0$, corresponding to $S_{-,c \rightarrow -\infty}(r)$, probability of $-3 \leq \tilde{u} \leq 0$, or $S_{-,c=3}(r)$, and of $-4 \leq \tilde{u} \leq 0$, or $S_{-,c=4}(r)$ are depicted, and compared with corresponding Gaussian values. This time, $G_{-,c=4}$ is practically indistinguishable from $1/2$. (d) The probability of $\tilde{u} \leq -3$ (or $S_{-,t=3}(r)$), and of $\tilde{u} \leq -4$ (or $S_{-,t=4}(r)$) are depicted in respect to their Gaussian values.

the intermediate range.

We now proceed to the analysis of the \pm moments. It is clear that there are several common features for ramp model and bump model, that is, common features in panels (c) and (e) of Fig. 1. As mentioned in Sec. II B, for both cases, $\langle \partial_x u \rangle = 0$ and $\langle (\partial_x u)^3 \rangle < 0$. This actually implies that the positive part of the distribution occupies larger space than the negative part. This is seen directly from panel (e), and can be calculated for the function depicted in panel (c), i.e. calculated directly from the function $\partial_x u_{st} + \partial_x u_\lambda$ defined in Sec. II B. In other words, $S_{-,c \rightarrow \infty}(r)$ should be less than $S_{+,c \rightarrow \infty}(r)$. As, on the other hand, $S_{-,c \rightarrow \infty}(r) + S_{+,c \rightarrow \infty}(r) = 1$, by definition, we have $S_{-,c \rightarrow \infty}(r) < 1/2$, and this quantity is typically increasing with growing r , while $S_{+,c \rightarrow \infty}(r) > 1/2$, decreasing with r . This is exactly what is observed in panel (c) of Fig. 6, although the curves are somewhat scattered. In spite of the latter, there is no doubt that $S_{-,c}(r) < S_{+,c}(r)$, for all distances and all values of c .

The box counting $S_{\pm,c=3}(r)$ and $S_{\pm,c=4}(r)$ behaves analogously. The intermediate range can be again distinguished in all of the curves depicted in panel (c), although the range is not that pronounced. This range can be better noticed from the tail moments, depicted in panel (d). It is clearly seen that the tails are stronger at small distances, and the intermediate range clearly noticeable. Besides, the negative distribution is definitely more singular than the positive, or $S_{+,t=3,4}(r) < S_{-,t=3,4}(r)$: and that is what is seen from this panel. This difference in singularity strength is obvious from the ramp model, Fig. 1(e), where the positive distribution is not singular at all. It is also seen from Fig. 1(c), that is, for the bump model, that the negative peak reaches higher absolute values than the positive peak, and therefore the negative singularity is expected to possess higher strength. Finally, again as in panel (b), the tails deviate quite substantially from Gaussian values for $t = 4$.

V. DISCUSSION OF THE MODEL

A. Intermittency formation

Let us return to the stretching process described in Sec. II A. In more general case of axisymmetric stretching we have,

$$\frac{\partial v_\phi}{\partial t} + \left[v_{r'} \frac{1}{r'} \frac{\partial r'}{\partial r'} + v_z \frac{\partial}{\partial z} \right] v_\phi = \nu \left[\frac{\partial^2}{\partial z^2} + \frac{\partial}{\partial r'} \frac{1}{r'} \frac{\partial}{\partial r'} r' \right] v_\phi. \quad (34)$$

In the vicinity of stagnation line $r' = 0$, this equation is reduced to (20) if operator $\nabla \times$ acts on (34). This equation is *linear* in respect to v_ϕ , and, if $v_{r'}$ and v_z are given, then the vortex stretching, described by equation (34) can be considered *kinematic*. In fact, this equation coincides with that for A_ϕ , ϕ -component of magnetic vector-potential, i.e., $B_{r'} = -\partial_z A_\phi$, $B_z = r'^{-1} \partial_{r'} r' A_\phi$, and \mathbf{B} is

magnetic field strength. The induction equation for A_ϕ , coinciding with (34), is kinematic if the velocity is given.

The equations for r and z -components of the velocity field read,

$$\begin{aligned} \frac{\partial v_{r'}}{\partial t} + \left[v_{r'} \frac{\partial}{\partial r'} + v_z \frac{\partial}{\partial z} \right] v_{r'} - \frac{v_\phi^2}{r'} = \\ - \frac{1}{\rho} \frac{\partial p}{\partial r'} + \nu \left[\frac{\partial^2}{\partial z^2} + \frac{\partial}{\partial r'} \frac{1}{r'} \frac{\partial}{\partial r'} r' \right] v_{r'} + F_{r'}, \end{aligned} \quad (35)$$

and

$$\begin{aligned} \frac{\partial v_z}{\partial t} + \left[v_{r'} \frac{\partial}{\partial r'} + v_z \frac{\partial}{\partial z} \right] v_z = \\ - \frac{1}{\rho} \frac{\partial p}{\partial z} + \nu \left[\frac{\partial^2}{\partial z^2} + \frac{\partial}{\partial r'} \frac{1}{r'} \frac{\partial}{\partial r'} r' \right] v_z + F_z, \end{aligned} \quad (36)$$

where ρ is density, and \mathbf{F} is external forcing.

In the vicinity of stagnation line $r' \rightarrow 0$ where there is the strain (19) motion plus the vortex, all the terms in equation (35) are functions of r' only, and therefore they can be compensated by the pressure. Analogously, all the terms in (36) are functions of z only, and again are compensated by the pressure. This means the “the cell”, i.e., the r and z -components of the velocity can be considered as given (and steady). In general, however, v_ϕ depends also on z , and therefore the third term in (35) gives nontrivial contribution to the equation. Nevertheless, as mentioned at the beginning of Sec. III, the velocity corresponding to the vortex is supposed to be small compared with the strain motion. In other words, the contribution of this term can be neglected. Besides, the external forcing is always able to make the cell steady. In any rate, if this term is neglected, then these two equations (35-36) are independent from existing vortex, and, from the point of view of the vortex generation, the $v_{r'}$ and v_z -components can be considered as given.

In this – somewhat simplified – picture, the vortex generation responsible for appearance of the intermittency, is kinematic, that is, passive. We may expect therefore that there is some analogy between this generation of intermittency and that of a passive scalar gradient. It is known that the latter is shown to be intermittent even if the background, that is, the given velocity is not [18].

Generally, we have the following energy balance equation,

$$\frac{d}{dt} \frac{\langle v^2 + v_\omega^2 \rangle}{2} = -\nu \langle (\nabla \times \mathbf{v})^2 + (\nabla \times \mathbf{v}_\omega)^2 \rangle, \quad (37)$$

where v_ω stands for the generated vortex. The first term on the right-hand-side corresponds to regular Kolmogorov cascade, and corresponding energy dissipation, and the second one – to the dissipation of the vortices. In the no intermittency model, Sec. II A, the second term is absent. On the contrary, in the extreme intermittency model Sec. II B, the first term can be neglected, because

of the large size of the cells, while the second makes up for the Kolmogorov dissipation if the initial amplitude of the vortex ω_ℓ is comparable with α_ℓ , see (29). In a more realistic model described at the beginning of Sec. III, both dissipation terms contribute. More specifically, the Kolmogorov cascade prevails, and the generated vortices give a small contribution to the dissipation (otherwise the intermittency is too strong). Let $\omega_\ell \approx f\alpha_\ell$, where $f < 1$, then

$$\nu \langle (\nabla \times \mathbf{v}_\omega)^2 \rangle \sim f^2 \frac{v_\ell^3}{\ell} \sim f^2 \varepsilon, \quad (38)$$

cf. (28). It is because of the smallness of f^2 that the process of vortex generation can be considered kinematic.

Presumably, the most vulnerable part of this picture is that the parameter f is essentially arbitrary. We can suggest some speculation about the origin of this parameter. Namely, the process of vortex formation, and vortex existence, are transitional. Indeed, the vortex cannot exist longer than the cell itself, where the vortex is generated. According to K41, a cell of the size ℓ exists only for a time $\sim \ell/v_\ell$. On the other hand, $1/\alpha_\ell \sim \ell/v_\ell$ as well. In other words, the vortex generation time, $1/\alpha_\ell$, and the life time of the cell, and therefore the life-time of the vortex itself, are comparable. Of course, these are just rough estimations. There is some dispersion both in the life-times, and in the generation times. We may expect, that a cell should be persistent, in order to have time enough to generate a vortex. That is to say that only a fraction of cells (which are persistent) would give rise to vortices. Another restriction arises from geometry. We may expect that there are vortex perturbations in each cell. However, as described in Sec. IIB, a cell would generate a vortex only if the initial perturbation is axisymmetric, with the axis parallel to the stagnation line of the cell. Generally, a perturbation, even with $\omega_\ell \approx \alpha$, would not be exactly the way described in Sec. IIB. Namely, it would not be expected to be axisymmetric at all. Considering again the interaction to be kinematic, we may expect that only axisymmetric part of the initial perturbation, – being generally a small fraction of the perturbation as a whole, – is transformed into a vortex, considered in Sec. IIA. Another solution to this problem can be seen in the fact that the generation of the vortices does not necessary proceeds in the largest cells. Of course, flatness according to (30) $\sim R$ is much too high. If, however, the generation proceeds from a cell of a size r , then, the flatness would be

$$F(0) \sim R_r = R \left(\frac{r}{\ell} \right)^{4/3} < R.$$

Another difficulty in this model is that it predicts the presence of intermittency only in the intermediate range, (32) in Sec. III. However, we can see from practically all the plots that the intermittency is present in the inertial range as well, although, being less intense. It can be seen, for example, from Figs. 4 and 5, where flatness

is depicted, that the latter has a decent scaling in the inertial range (for two decades!). Nontrivial behavior in inertial range can be also observed in Fig. 6, especially in panels (a) and (b). The tail events are particularly noticeable for the tails with $t = 4$, and their deviation from Gaussian is substantial in numbers, as seen from panel (b), although these events are less pronounced than in intermediate range (and the curve is more scattered).

We may suggest the following explanations. First, as noted above in this section, the vortices are transitional events, being generated at large scales, and then, with diminishing scales they reach their final scale λ . Thus, at some point in time, each vortex has a size comparable with r , and therefore it may contribute to the distribution. Second, strictly speaking, the structures of smaller (and larger) than r scales do contribute to the structure functions taken at a distance r . Therefore one may expect that the structure functions for distances r corresponding to the inertial range would reflect the intermittency of smaller scales, or possibly the intermittency of the intermediate range only.

B. Ramp model versus bump model

As we noticed in previous section, there are several common features between these two models. Here, we focus on differences. First, the estimates (26-27) differ for the ramp model. The first moment is still zero, of course, $\langle \partial_x u_{ramp} \rangle = \omega \cdot (r - \delta) - [(r - \delta)/\delta] \omega \cdot \delta = 0$. Here δ is the size occupied by the negative part, and therefore $r - \delta$ corresponds to the remaining positive part, the amplitude of the positive part being ω , see Fig. 1(e). The third moment is negative. Indeed,

$$\langle (\partial_x u_{ramp})^3 \rangle = \omega^3 (r - \delta) - \left(\frac{r - \delta}{\delta} \omega \right)^3 \delta < 0 \quad (39)$$

which is negative if $\delta < r$. Therefore, the skewness is negative as in (26-27), but the parameters entering this expression are different.

The main conclusion about the ramp model is that the strength of the negative singularity is higher than that of the positive,

$$D_q^- < D_q^+, \quad (40)$$

where D_q^\pm are generalized dimensions, [7]. In the simplified picture illustrated in Fig. 1(e), the positive part is not singular at all, that is, $D_q^+ \equiv 1$. On the other hand, the bump model does suggest that the positive part is singular, although the inequality (40) is satisfied: it is seen from Fig. 1(c), and follows from discussion at the end of previous section. The singularity of positive tails is indeed observed, see Fig. 6(d), and that may be considered as a preference of the bump model as compared with the ramp model.

Generally, the bump model can be considered as a more subtle and sophisticated version of the ramp model,

the former suggesting essentially the same predictions as the latter. Obviously, the ramp model is purely empiric, while the bump model describes some dynamical processes in formation of vortices. Indeed, Fig. 1(f) presents two ramps, one is what is expected, and another one (dashed-dotted line) corresponds to a statistically unlikely ramp. This statistical preference is so far not understood. It was suggested in [7] that the situation is analogous to a shock wave formation: a shock would never develop in the shape like depicted with a dashed-dotted line, and it evolves only into “real ramp”, (solid line). This analogy is of little help, however, the typical turbulence being incompressible, and the shocks are therefore irrelevant. On the other hand, the bump should appear on descending part of the curve, where the derivative is negative, as depicted in Fig. 1(d), solid line, as opposed to “unrealistic” bump depicted with dashed-dotted line. This statistical preference can be explained, as opposed to the ramp-model statistics. Indeed, the ascending part of the curve (with positive derivative) corresponds to a structure function with vector \mathbf{r} parallel to the vertical direction, where the derivative ($= 2\alpha$) is indeed positive, while the descending part corresponds to \mathbf{r} in horizontal plane (where the derivative is $= -\alpha < 0$). Now, the bump corresponds to the vortex, and, of course, the corresponding velocity is suited in the horizontal plane. Therefore, the bump would appear only on descending part of the curve.

Finally, let us discuss the quantitative estimates for the asymmetry. As mentioned in Sec. II A, the non-intermittency scenario does not account for the asymmetry. The latter is easily explained in extreme intermittency approach, see Sec. II B. The corresponding expression (27) does provide a realistic estimate of the skewness, as noted at the end of II B. However, this estimate corresponds to extreme intermittency scenario, i.e., to *unrealistic intermittency*. Still, the asymmetry can be explained if we suggest that the vortex formation proceeds all the time. That is to say that the transitional stage mentioned in previous subsection is always present. If there is enough time for the perturbation to reach the Taylor microscale, then the vortex is complete, and therefore the intermittency is generated. But, considering the fact that the intermittency is not that pronounced in fully developed turbulence, we conclude that the final formation of a vortex is a relatively rare event. More often, the vorticity of a perturbation is enhanced for a while, and then the generating cell ceased to exist, and thus the generation stops. However, during this amplification, the vorticity of the generated vortex easily exceeds the causing this generation strain, and then, according to (26), the third order structure function becomes negative. This is valid for any particular scale r , if the vortex reaches it (and its vorticity exceeds the strain). This may account for the Kolmogorov law.

VI. CONCLUSION

It is known that production of vorticity, or vortex stretching, does not necessary implies that intermittency is generated. Indeed, in classical Kolmogorov picture K41, the energy cascade from large eddies to small actually implies that small scale vortices are generated: because the vorticity production proceeds homogeneously. In other words, each eddy decays into smaller eddies, *each of which* in turn decays into smaller eddies, and so on.

As we argued above, the vortex stretching may be considered as kinematic, in some limited sense, of course. For a passive scalar ψ , the classical Kolmogorov picture is not much different from what is described in the previous paragraph. That is, ψ^2 is transported down the scales, so that $\langle (\nabla\psi)^2 \rangle$ is growing (which is similar to the vorticity production). The energy cascade is gradual and continuous in this picture, meaning that the large scale fluctuations generate smaller scale perturbations, which in turn generate even smaller scales, and so on, until the perturbations reach diffusive scale where they eventually disappear. We can imagine a *direct* cascade of energy, without passing the intermediate scales in inertial range, directly from the large scales to the dissipation scale. To be more specific suppose, that the velocity turbulence is presented by large scale cells only (of the size ℓ): like in Sec. II B, but the velocity field is random in time, unlike time-independent, i.e., steady cells from Sec. II B. Generally, maxima of $\nabla\psi$ will be generated in the vicinity of the stagnation lines and stagnation surfaces, in a time-scale $\sim \ell/v_\ell$. The $\nabla\psi$ -field will have the scale of Taylor microscale. However, if the life-time of the eddies $\tau_\ell \approx \ell/v_\ell$, as in regular turbulence, then, first, there would not be enough time to produce a sharp and concentrated structure of the $\nabla\psi$ -field during one turn-over time, and second, in the next life-time, the concentrated $\nabla\psi$ -field structure is formed in a different place. As a result, the $\nabla\psi$ -field is generated homogeneously in statistical sense. In other words, there is no intermittency generated. Suppose now that the turbulent cells are persistent, or, at least, some of them are. Then, distinct $\nabla\psi$ -field structures are generated, and they are as persistent as the cells themselves. The scenario described in Sec. II B of vortex generation is essentially the same.

We presented an evidence of the presence of vortices in high Reynolds turbulence. This is clear from the figures: the intermediate scale range (32), where these vortices are supposed to appear (see the beginning of Sec. III, and also [5]), is clearly noticeable. The main feature which distinguishes this range is a substantially enhanced intermittency. The vortices are aligned to the intermediate eigen-vectors, [6], [5], [17]. And, most important, these vortices account for negative skewness, that is, they result in a right asymmetry of the PDF. This picture promoted a development of the ramp model which is modified now into the bump model. The latter not only explains more features than the former, but also the bump

model seems to be dynamically substantiated, unlike the ramp model, see Sec. VB.

The most important conclusion is that the intermittency is related to the asymmetry of statistical properties of turbulence, which was suggested in [7]. This gives us a powerful tool for studying the intermittency: because the asymmetry is manifested in lower moments of structure function, while the intermittency normally manifests itself in higher moments with poor statistics.

Still, the whole picture is far from complete. As mentioned in Sec. III, this simple scenario, outlined again above in this section, predicts too much intermittency. There are some suggestions in Sec. III as to how to cure this difficulty. But, so far, the theory is unable to predict *the numbers*, e.g., we cannot predict the flatness from the asymmetry, or the other way. Nevertheless, we believe that the paper provides a next step in understanding the intermittency of turbulence.

ACKNOWLEDGMENTS

I thank K. R. Sreenivasan and B. Dhruva for the data of high Reynolds number atmospheric turbulence used in this paper. I also appreciate discussions with W. Goldberg, J. Gollub, X. L. Wu, and Z. Warhaft.

- [15] A. A. Townsend, Proc. R. Soc. London A, **208**, 534 (1951); D. I. Pullin and P. G. Saffman, Phys. Fluids A **5**, 126 (1993).
- [16] R. Betchov, J. Fluid Mech., **1**, 497 (1957).
- [17] T. Dracos, M. Kholmyansky, E. Kit, and A. Tsinober, in *Topological Fluid Mechanics*, edited by H. K. Moffatt and A. Tsinober (Cambridge U. P., Cambridge, 1989).
- [18] Z. Warhaft, Annu. Rev. Fluid Mech., **32**, 203, (2000).

-
- [1] S. Le Dizès, M. Rossi, and H.K. Moffatt, Phys. Fluids, **8**, 2084 (1996).
 - [2] H.K. Moffatt, S. Kida, and K. Ohkitani, J. Fluid Mech, **259**, 241 (1994).
 - [3] J. Jiménez, Phys. Fluids A, **4**, 652 (1992); S. Kida, *Lecture Notes in Numerical Applied Analysis*, **12**, 137 (1993).
 - [4] N. Hatakeyama and T. Kambe, Phys. Rev. Letters, **79**, 1257 (1997).
 - [5] A. Vincent and M. Meneguzzi, J. Fluid Mech, **225**, 1 (1991).
 - [6] R. M. Kerr, J. Fluid Mech., **153**, 31 (1985); W. T. Ashurst, A. R. Kerstein, R. M. Kerr, and C. H. Gibson, Phys. Fluids, **30**, 3243 (1987).
 - [7] S.I. Vainshtein and K.R. Sreenivasan, Phys. Rev. Lett., **73**, 3085 (1994).
 - [8] A.N. Kolmogorov, C.R. Acad. Sci. U.S.S.R. **32**, 16 (1941).
 - [9] S.I. Vainshtein, Phys. Rev. E, **56**, 6787 (1997).
 - [10] S.I. Vainshtein, Phys. Rev. E, **58**, 1851 (1998).
 - [11] S. I. Vainshtein, Phys. Rev. E, **61**, 5228 (2000).
 - [12] A.N. Kolmogorov, C.R. Acad. Sci. U.S.S.R. **30**, 301 (1941).
 - [13] A.S. Monin and A.M. Yaglom, *Statistical Fluid Mechanics*, Vol. 2 (MIT Press, Cambridge, Mass, 1971)
 - [14] H. Tennekes and J.L. Lumley, *A First Course in Turbulence*, (MIT Press, Cambridge, Mass., 1972).